Supplementary Information

Cation- and pH- dependent hydrogen evolution and oxidation reaction kinetics

Botao Huang*[1,2], Reshma R. Rao[1,2], Sifan You[6], Kyaw Hpone Myint[3], Yizhi Song[6], Yanming Wang[2], Wendu Ding[3], Livia Giordano[1,2], Yirui Zhang[1,4], Tao Wang[1,2], Sokseiha Muy[1,2], Yu Katayama[1,7], Jeffrey C. Grossman[5], Adam P. Willard[3], Kang Xu[8], Jiang Ying[6] and Yang Shao-Horn*[1,4,5]

[1] Electrochemical Energy Laboratory, [2] Research Laboratory of Electronics, [3] Department of Chemistry, [4] Department of Mechanical Engineering, [5] Department of Material Science and Engineering, Massachusetts Institute of Technology, 77 Massachusetts Avenue, Cambridge, MA 02139, USA

[6] International Center for Quantum Materials, School of Physics, Peking University, Beijing 100871, People's Republic of China

[7] Department of Applied Chemistry, Graduate School of Sciences and Technology for Innovation, Yamaguchi University, Ube 755-8611, Japan

[8] Battery Science Branch, Sensor and Electron Devices Directorate, U.S. Army Research Laboratory, Adelphi, Maryland 20783-1197, USA

Corresponding Author*

E-mail: huang73@mit.edu

E-mail: shaohorn@mit.edu

Table of content

Methods

Classical molecular dynamic (MD) simulations

To isolate the effect of pH on the cation-electrode binding affinity, we set up a series of simulations of an aqueous electrolyte solution of Cl^- and alkali ions (Li^+, Na^+, K^+, Rb^+, Cs^+) confined between platinum electrodes at constant potential of -0.3 V and at -1.1 V relative to PZC for Pt(111) surface, corresponding to 0 V_{RHE} at pH 1 and pH 13 respectively. As we study the negative charged Pt(111) surface, where cations were expected to interact with the surface by Coulombic interaction. Due to limited validation of the force field parameters of ClO_4^- and OH^- anions, Cl- anions were considered to replace ClO_4^- for simulating acidic solutions and OH^- for simulating alkaline solutions. All the simulations were performed in LAMMPS. A simulation box with dimensions of 30.43 x 28.75 x 89.23 Å was periodically replicated in *x,y*-directions while fixed boundary condition was employed for the z-direction containing the platinum electrode. The simulation box contained 792 Pt atoms, 2293 water molecules and 42 alkali ions with equal amount of Cl^- anion as their counter ions, approximately corresponding to a 1 M concentration of cations. Due to the lack of appropriate force field parameter to describe proton and hydroxyl in the literature, Cl^- ions were used as counter ions to balance the charge of alkali metal cations for both pH1 and pH13. The long-range electrostatic interactions[32] were calculated by using a Particle-mesh Ewald algorithm with a real-space cut off value of 9 Å. An NVT ensemble with Langevin thermostat was employed to keep the system at 300 K. Langevin thermostat was used here as we were only concerned with the statics properties of the system at equilibrium. Furthermore, the Shake algorithm[33] was used to constrain the bonds and angles of SPC/E water. The system was equilibrated for 0.1 ns before performing the final production runs of 1 ns with time step of 2 fs using the SPC/E force field for water. Lennard-Jones (LJ) parameters were used along with the scaled-ionic-charge model for alkali ions, in order to account for electronic polarization effects in a classical non-polarizable force field. Lorentz-Berthelot mixing rules were employed to derive the mixed Lennard-Jones parameters. The Pt(111) electrode atoms were modelled using the LJ forcefield from Ref. [34]. The charges on each platinum atoms were calculated at each time step to satisfy the imposed voltage across the cell (either 0.3 or 1.1 V) by the constant potential fix in LAMMPS developed by Wang et al.[35] All the parameters used are summarized in Table S1. Note that our MD simulation system did not include the presence of H_{ad} on Pt surface at 0 V_{RHE}. As a result, the simulations are of limited quantitative value. However, we assume that qualitative trends that emerge when changing cation identity are physically meaningful. While our simulations did not include the potential difference in the relative surface hydrophobicity, or the associated changes in the double layer water structure, the free energy differences in the cation desolvation responsible for the cation-dependent trends in interfacial structure were expected to be similar for both hydrophilic (without H_{ad}) and hydrophobic (with H_{ad}) surfaces as cation-dependent interfacial water structure on hydrophobic surface (CO covered Pt) has also been reported previously.[36] While the exact interfacial water structure in our MD simulation might be different from realistic condition, our MD simulation results via the simplified model are supported by our reorganization energy, reaction entropy and *in situ* SEIRAS experiments. Further study by considering H_{ad} on Pt surface in MD simulation is needed to provide more quantitative information.

Electrochemical measurements and electrolyte preparation

A Biologic SP-300 potentiostat and a three-electrode electrochemical system[37] were employed for all electrochemical measurements. A Pt rotating disk electrode (RDE) (Pine instrument) was used as the working electrode. Potentials were recorded versus a mercury sulfate ($Hg/HgSO_4$)

reference electrode in acidic and buffer solutions and to a mercury oxide (Hg/HgO) reference electrode in alkaline electrolytes. All potentials were converted to the RHE scale. The effects of pH and cations on H adsorption and the kinetics of HER/HOR were examined by CV measurements at a scan rate of 50 mV s^{-1} in Ar saturated electrolytes and 10 mV s^{-1} in H_2 saturated solutions at 293 K. The normalized current density was obtained using the geometric surface area of RDE (0.196 cm^2) and the reported potentials were iR corrected. For temperature dependent measurements, the cell temperature was controlled by a thermal bath circulator (Thermo Neslab RTE 7) and increased from 293 to 323 K in increments of 10 K. Buffer solutions, acidic and alkaline electrolytes were prepared from deionized water (Millipore, >18.2 MΩ.cm). For cation-dependent measurements, 0.1 M perchlorate salt of Li^+, Na^+, or 0.08 M perchlorate salt of K^+, Cs^+ or 0.05 M perchlorate salt of Rb^+ were added to electrolyte at pH 1 and pH 2 prepared by diluting $HClO_4$ (Sigma-Aldrich 70 wt%). Alkaline electrolytes at pH 12-14 were prepared with aqueous solutions of 0.01-1 M lithium hydroxide (Sigma-Aldrich 99.9%), sodium hydroxide (Sigma-Aldrich 99.9%), potassium hydroxide (Sigma-Aldrich 99.95%), rubidium hydroxide (Sigma-Aldrich 99.95%) and cesium hydroxide (Sigma-Aldrich 99.95%). The purity of cesium hydroxide was further analyzed by inductively coupled plasma (Table S2). Buffer solutions were prepared by adding different amounts (e.g. 1 and 2 ml) of 4 M hydroxide of Li^+, Na^+, K^+, Rb^+ and Cs^+ into 50 ml of 0.2 M solution of phosphoric acid (Sigma-Aldrich 80 wt%), citric acid (Sigma-Aldrich 99.9%) and acetic acid (Sigma-Aldrich 99.9%), bicarbonate (Sigma-Aldrich 99.9%) and carbonate (Sigma-Aldrich 99.9%).

For the extraction of kinetic current density, we measured HER/HOR polarization curves with Pt RDE at rotation speeds from 400 to 2500 rpm, as shown in Figs S1a-c. Kinetic current density could be estimated from rotation speed dependent HOR polarization curves using the Koutechy-Levich equation.[38]

$$\frac{1}{j} = \frac{1}{j_k'} + \frac{1}{j_L} = \frac{1}{j_k'} + \frac{1}{0.62nFA'D_O^{2/3}\omega^{1/2}\nu^{-1/6}C_O^*} \qquad \text{Eq. (S1)}$$

where j denotes measured current density; j_k' is the kinetic current density from the slow kinetic model; j_L is the limiting current density; n is the number of electrons transferred during the reaction; F is the Faraday constant; A' is the surface of electrode; D_O and C_O^* are the diffusion coefficient and bulk concentration of oxidant; ν is the cinematic viscosity of the electrolyte; ω denoted rotation rate. The expression (Eq. S1) assumes that 1) the redox process is a reversible and the reaction is first order; 2) the electron transfer rate is slow (e.g. $j_k'/j_L < 0.1$) and governed by kinetics rather than mass transport, where the current is described by $j = FA'k_f(E)C_O(y = 0)$, having y as the distance from the electrode surface. On the other hand, for electrochemical reactions in fast kinetics (e.g. $0.1 < j_k'/j_L < 1$), the current could be limited by mass transport event at low overpotential, $j = nfA'D_O[C_O^* - C_O(y = 0)]/\delta_O$, with δ_O denoting the diffusion layer thickness of the oxidant at an electrode. In this regime, the following expression can be more accurate for Koutechy-Levich analysis: [7]

$$\frac{1}{j} = \frac{1}{FA'\left(k_f C_O^* - k_b C_R^*\right)} + \frac{D_O^{-2/3}k_f + D_R^{-2/3}k_b}{0.62\nu^{-1/6}\omega^{1/2}} = \frac{1}{j_k} + \frac{D_O^{-2/3}k_f + D_R^{-2/3}k_b}{0.62\nu^{-1/6}\omega^{1/2}} \qquad \text{Eq. (S2)}$$

D_R denotes the diffusion coefficient of reductant; k_f and k_b are the rate constants of forward and backward reactions, respectively. For example, HER/HOR kinetics on Pt in aqueous solutions containing 0.1 M hydroxides, were slow ($j_k'/j_L < 0.1$) for overpotential range within few millivolts for both oxidation and reduction, which was too narrow to explore kinetic parameters using electron transfer theories (Figs S1g-i). Moderate and fast kinetics regions ($0.1 < j_k'/j_L < 1$) were located at overpotential range up to 30-60 mV (e.g. 30 mV for Li^+, Na^+ and Cs^+, 60 mV for K^+, Figs S1g-i), where the fast kinetic model (Eq. S2) could be more suitable for the extraction of kinetics current.

To extract kinetic parameters, including the exchange current density and reorganization energy, from kinetic current density, the Butler-Volmer equation and MHC formalism[8,9] were employed. In addition, the microscopic MHC formalism that accounts for the quantum mechanical nature of electron transfer and the solvent reorganization energy of the solvation shell and the electron energy levels in metal electrode, was fitted to the HER/HOR kinetics current density, $j_{red/ox}^{MHC}$ with the following expressions:

$$j_{red/ox}^{MHC}(\eta) = A\int_{-\infty}^{\infty} exp\left(-\frac{(x-\lambda\pm e\eta)^2}{4\lambda k_B T}\right)\frac{dx}{1+exp(x/k_B T)} \quad \text{Eq. (S3)}$$

$$A = \frac{2\pi H_{AB}^2}{h(4\pi\lambda k_B T)^{1/2}} \quad \text{Eq. (S4)}$$

where λ is reorganization energy, k_B is Boltzmann constant, T is temperature, η is the over potential, A is the pre-exponential factor, [10,11] accounting for the electronic coupling strength where h is the Plank constant, H_{AB} is the electronic coupling energy. The electronic density of states (DOS) of the electrode, x accounts for the Fermi statistic of electron energies distributed around the electrode potential. The first term in the integrand is the classical Marcus rate for the transfer of an electron of energy x relative to the Fermi level, and the second factor is the Fermi-Dirac distribution assuming a slowly varying DOS, which to first approximation can be considered uniform. The corresponding exchange current density, j_0 can be calculated as following equation. [8]

$$j_0 = \frac{2\pi H_{AB}^2}{h\sqrt{4\pi\lambda k_B T}}\frac{\sqrt{\pi\lambda}}{2} erfc\left(\frac{\lambda-\sqrt{1+\sqrt{\lambda}}}{2\sqrt{\lambda}}\right) \quad \text{Eq. (S5)}$$

The MHC formalism, widely employed to accurately predict activity trends of numerous Faradaic reaction kinetics, including inner-sphere and outer-sphere reactions, for example, PCET reactions (HER/HOR on nickel-based molecular electrocatalyst[12] and the reduction of water-superoxide ion complex on glassy carbon electrode[13]), interfacial ET on the metal surfaces,[14] lithium electrodeposition/stripping[15] and lithium-ion intercalation at solid-solid interfaces,[9,16] considers the reactant-solvent interactions but not the reactant-electrode interactions (Appendix S1), which can be used to describe the HER/HOR kinetics on Pt as the hydration energy of proton (-11.5 eV)[17] is two orders of magnitude larger than HBE on Pt (-0.1 eV).[18] This hypothesis is supported by the fact that the values of exchange current density extracted by MHC formalism (Figs S2a,c) are comparable to those extracted via Butler-Volmer equation (Figs S2b,c). Further support comes from that the values of the reorganization energy of the Volmer reaction on metal surface has been reported to be ~0.4 eV,[19] which is comparable to the cation-dependent reorganization energy found in this work, 0.6-1.2 eV. Therefore, based on our learnings from the literature (refs [13,20–22]) and the consistency between our results and previous work (refs [23,19]), we propose that the kinetics of HER/HOR on Pt RDE can be described by the MHC formalism.

The MHC formalism also includes the standard free energy of activation, which consists of the inner-sphere and outer-sphere contributions arising from the structural reorganization of the reactants and the surrounding solvent. The solvation free energy of reactants is largely based on Born model, assuming that the solvent is a dielectric continuum, and each reactant is treated as a sphere, having the first solvation layer dielectrically saturated.

The free energy of activation $\Delta G^{\neq}$ of the HER/HOR was estimated from temperature dependent exchange current density via Arrhenius equation [24]:

$$j_0 = A\cdot exp\left(-\frac{\Delta G^{\neq}}{RT}\right) \quad \text{Eq. (S6)}$$

where $\Delta G^{\neq}$ is the free energy of activation. The free energy of activation obtained by Arrhenius approach was compared to the reorganization energy from the MHC formalism (Eqs S3-5).

In situ Surface-Enhanced Infrared Absorption Spectroscopy (SEIRAS)

A hemispherical Si prism (radius 22 mm, Pier optics) deposited with Pt was mounted in a spectro-electrochemical three-electrode cell. The reference electrode used was a mercury oxide electrode and a platinum-wire was used as the counter electrode. A Fourier-Transform Infrared (FTIR) Vertex 70 (Bruker) spectrometer equipped with an MCT detector was used to record SEIRAS spectra. The optical path was fully replaced with N_2 gas. The SEIRAS spectra were obtained with 4 cm^{-1} resolution at 7.5 kHz scan velocity in the 500 - 4000 cm^{-1} spectral range; 64 scans were averaged. The SEIRAS spectra were recorded using a single reflection ATR (Attenuated Total Reflection) accessory (Pike Vee-Max II, Pike Technologies) with a Si prism at an incident angle of 68°. Additional experimental details for the *in situ* SEIRAS measurements can be found elsewhere.[25,26] For *in situ* SEIRAS measurements during HER/HOR in electrolyte at pH 13, electrolytes consisted of 0.1 M hydroxide of Li^+, K^+ and Cs^+ were saturated with H_2 by purging H_2 gas. Before *in situ* SEIRAS measurements, the prism surface was cleaned by cycling the potential between 0.05 and 1.1 V_{RHE}. SEIRAS spectra were collected at potential from 1.1 to -0.3 V_{RHE} at room temperature. The reference spectrum I_0 was measured at 1.1 V_{RHE}. All spectra are shown in absorbance units defined as $\log(I_0/I)$, where I_0 and I represent the spectra at the reference and sample potentials, respectively. We note that the same Pt surface was used for measurements in 0.1 M LiOH, KOH and CsOH to ensure a similar surface enhancement effect.

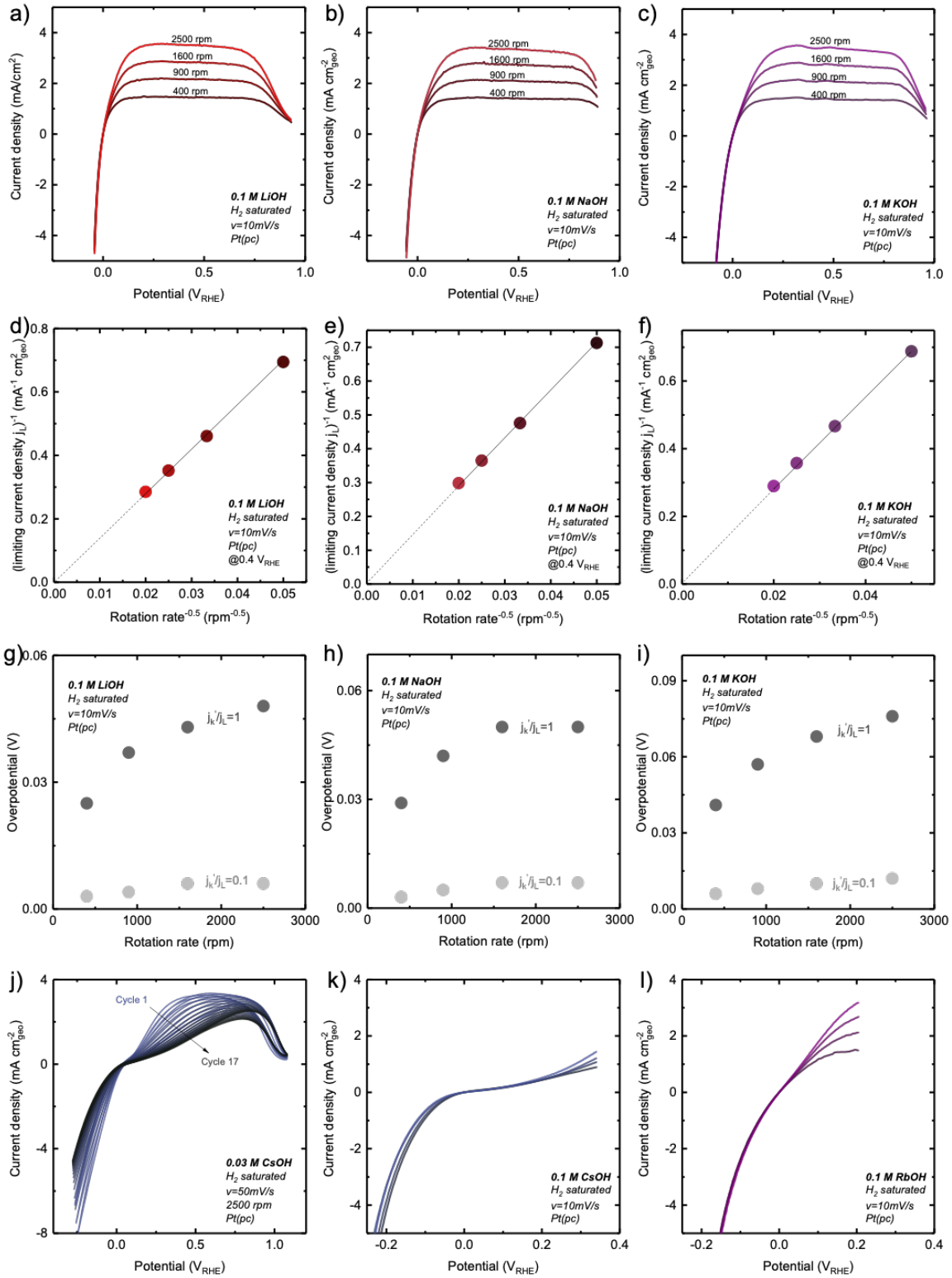

Figure S1. Cyclic voltammograms (CV) of HER/HOR measured on Pt RDE at rotation speed of 400, 900, 1600, 2500 rpm measured at 10 mV s^{-1} in H_2-saturated aqueous solution at 293 K and pH13 containing 0.1 M hydroxide of (**a**) Li^+, (**b**) Na^+, (**c**) K^+. Koutechy-Levich plot of the reciprocal of transport-limiting currents (measured at 0.4 V_{RHE}) $1/j_L$ against (rotation rate)$^{-0.5}$ for (**d**) Li^+, (**e**) Na^+ , **(f)** K^+ cases. Ratio of kinetic current density over limiting current density j_k'/j_L, where j_k' was estimated from Koutecky-Levich equation $1/j_{meas} = 1/j_k' + 1/j_L$ and j_L was estimated from plateau value in CV (Fig. S1), for **(g)** LiOH, **(h)** NaOH, **(i)** KOH. **(j)**

HER/HOR Polarization curves in H_2-saturated aqueous solution at 293 K and pH13 containing 0.1 M hydroxide of Cs, showing that the measurement current density decreases with cycle numbers, which could be attributed to the irreversible sub-surface oxidation of Pt for potential above 0.6 V_{RHE}.[27] To avoid the irreversible sub-surface oxidation of Pt, HER/HOR polarization curves were measured below 0.3 V_{RHE} for **(k)** Rb^+ and 0.2 V_{RHE} for **(l)** Cs^+.

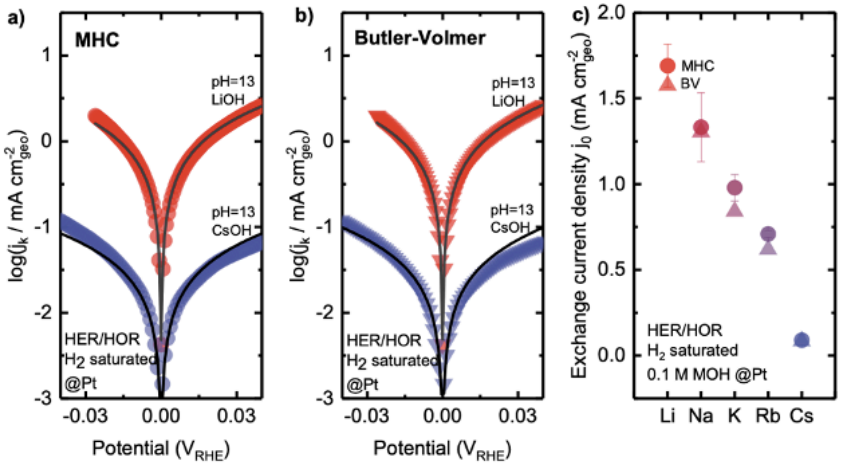

Figure S2. Fitting of kinetic currents of HER/HOR measured on Pt RDE surface in the electrolyte of 0.1 M LiOH and 0.1 M CsOH by **(a)** Marcus-Hush-Chidsey (MHC) theory and **(b)** Butler-Volmer (BV) equation. **(c)** Comparison of exchange current density extracted by MHC (circle) and BV (triangle) in H2 saturated electrolytes of 0.1 M hydroxide of Li^+, Na^+, K^+, Rb^+ and Cs^+ at 293 K.

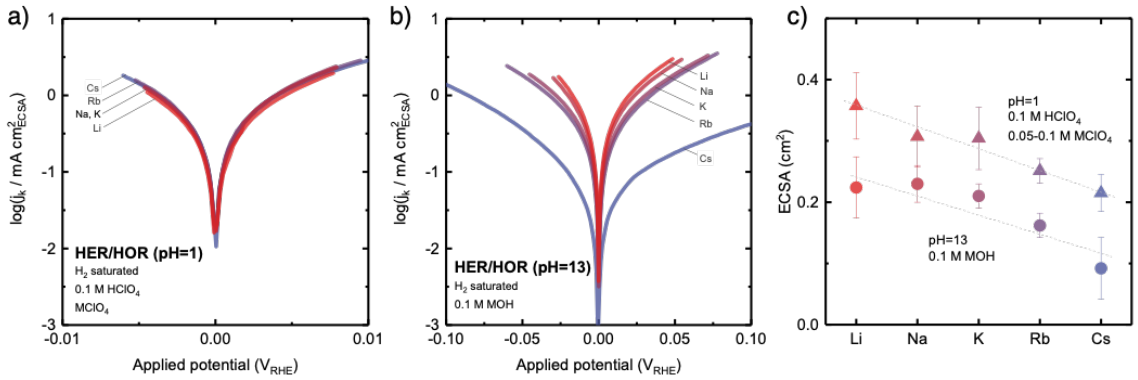

Figure S3. Cation effect on the kinetics current density normalized by ECSA of HER/HOR kinetics on Pt RDE at (a) pH=1 in H_2-saturated 0.1 M $HClO_4$ and 0.1 M $LiClO_4$, $NaClO_4$, or 0.08 M $KClO_4$, $RbClO_4$, or 0.05 M $CsClO_4$, and (b) pH=13 in H_2-saturated 0.1 M LiOH, NaOH, KOH, RbOH, CsOH. Note that the HER/HOR current density on Pt at pH 1 is hindered by mass transport and the kinetics cannot be separated from diffusion current density. (c) cation dependence of ECSA at pH1 and pH13 estimated from the desorption of H_{UPD} features of CV measured in Ar-saturated electrolyte, shown in Fig. S9. Error bars were obtained from the standard deviation of 3 independent measurements.

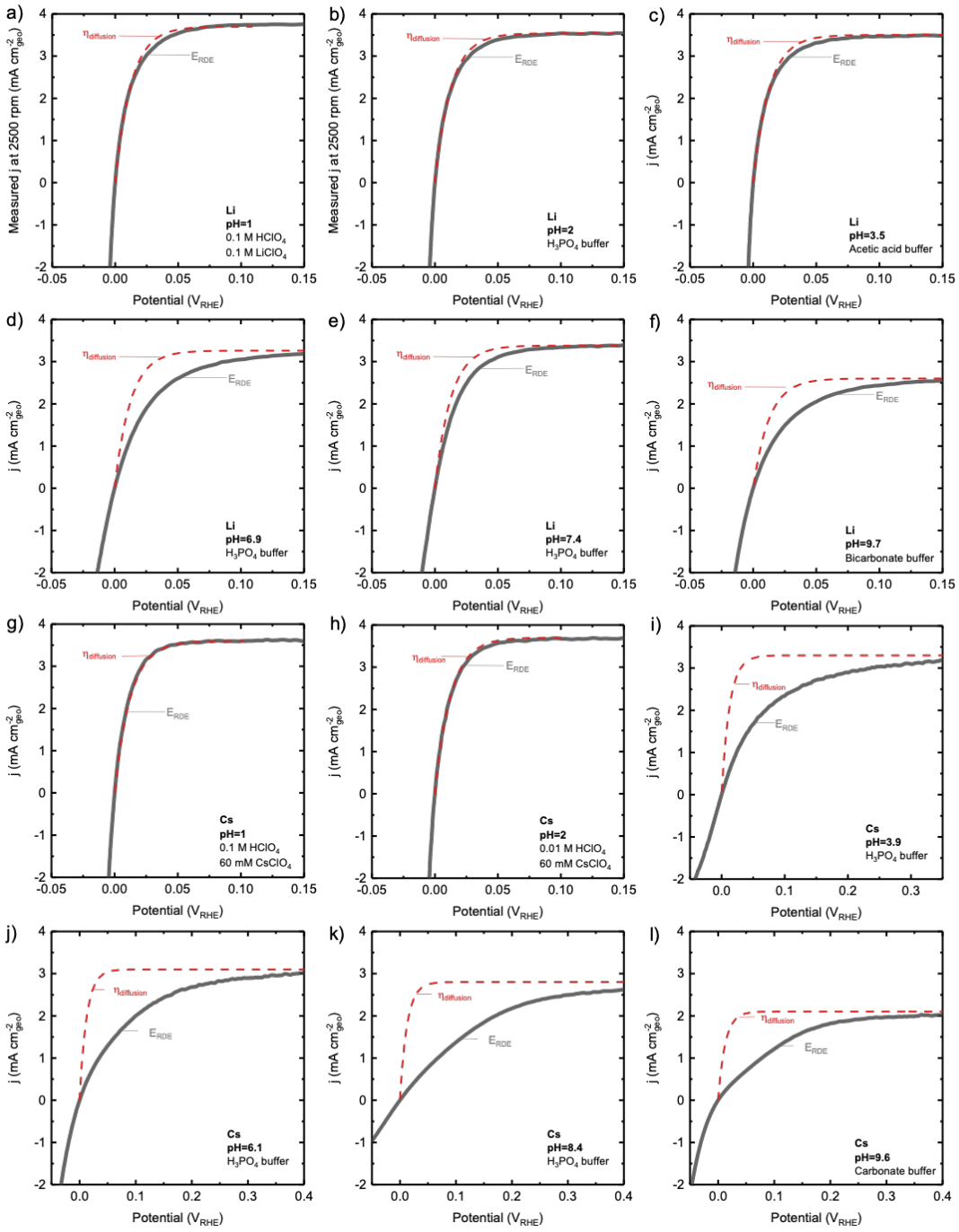

Figure S4. Calculated Nernstian diffusion overpotential[28] and measured HER/HOR polarization curves in electrolyte at various pH are compared to identify the critical point (minimum pH or maximum exchange current density) for which kinetic current density is able to be extracted from measured current density by Koutechy-Levich equation. HER/HOR polarization curves measure at 2500 rpm (black solid) and corresponding Nernstian diffusion overpotential (red dash) are plotted for aqueous electrolytes containing Li^+ at (a) pH 1, (b) pH 2, (c) pH 3.5, (d) pH 6.9, (e) pH 7.4, (f) pH 9.7, and for aqueous electrolytes containing Cs^+ at (g) pH 1, (h) pH 2 (i) pH 3.9, (j) pH 6.1, (k) pH 8.4, (l) pH 9.6. We found that for pH >6.9 (**Fig. S4d**) for Li^+ and pH>3.9 **(Fig. S4i**) for Cs^+, the Nernstian diffusion overpotential and experimentally measured current density were distinguishable, where the critical values of exchange current density is ~6 mA cm^{-2}.

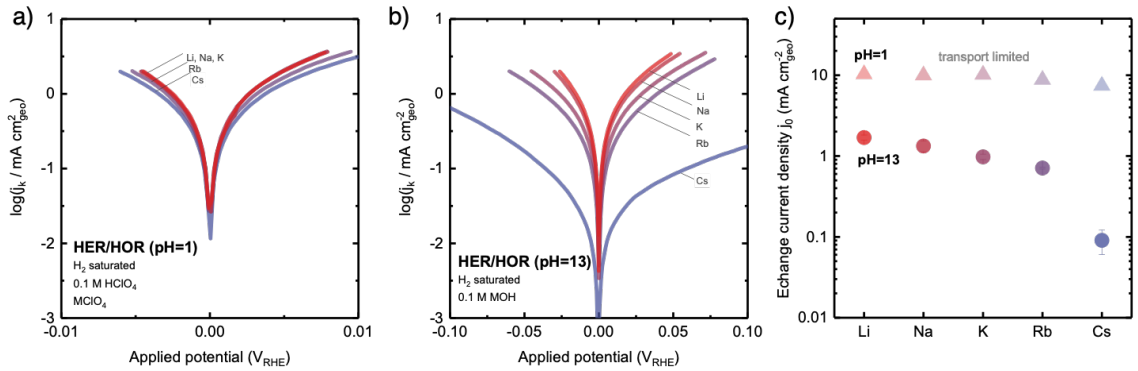

Figure S5. Cation effect on the kinetics current density normalized by geometric surface of HER/HOR kinetics on Pt RDE at (a) pH=1 in 0.1 M $HClO_4$ and 0.1 M $LiClO_4$, $NaClO_4$, or 0.08 M $KClO_4$, $RbClO_4$, or 0.05 M $CsClO_4$, and (b) pH=13 in 0.1 M LiOH, NaOH, KOH, RbOH, CsOH. (c) Exchange current density extracted by fitting MHC formalism. Note that as shown in **Fig. S4**, the HER/HOR current density on Pt RDE at pH 1 is hindered by mass transport and the kinetics cannot be separated from diffusion current density, thus the exchange current density at pH1 shown in **Fig. S5c** does not reflect to the pure HER/HOR kinetics at pH1.

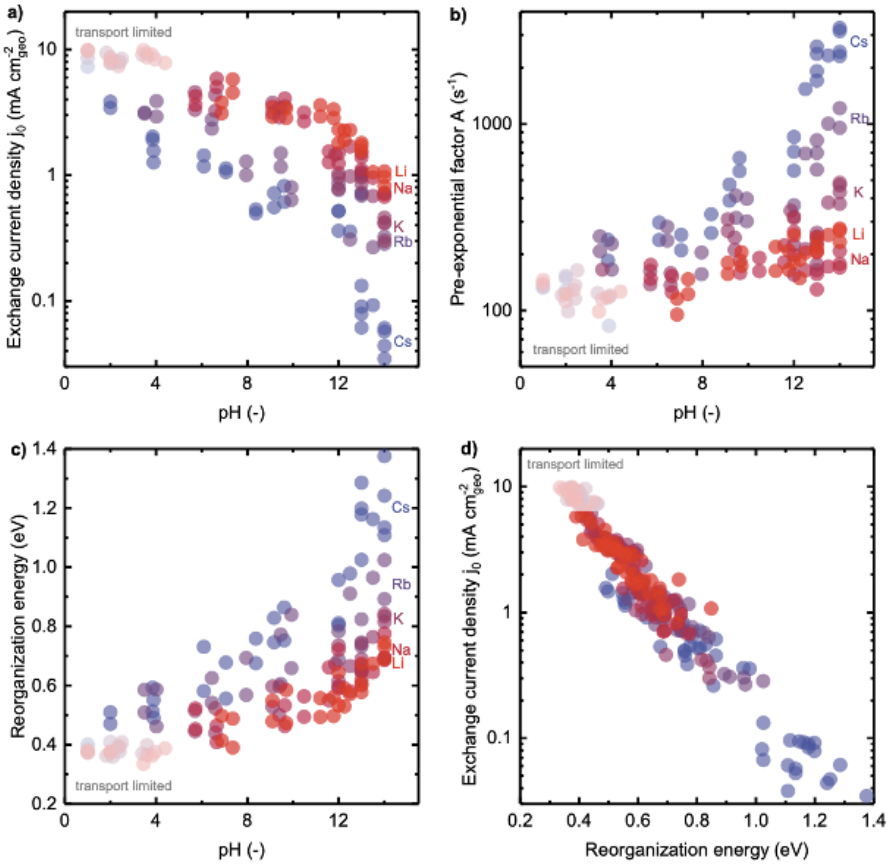

Figure S6. Extraction of reorganization energy of HER/HOR on Pt electrode from MHC formalism with full data points of 2-3 independent measurements. (a) exchange current density j_0, **(b)** pre-exponential factor A, **(c)** reorganization energy extracted by MHC formalism, **(d)** exchange current density plotted against reorganization energy. Mass transport limitation in Pt RDE measurements underestimates the exchange current density > ~6 $mA\ cm^{-2}_{geo}$, which is shaded (Fig. S4).

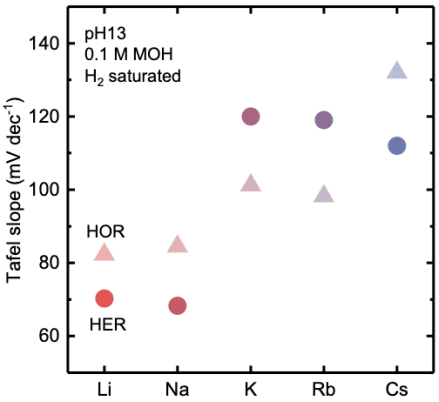

Figure S7. Tafel slope of HER/HOR kinetics current density on Pt RDE normalized by geometric surface, measured in H_2-saturated aqueous solutions at pH13 of 0.1 M LiOH, NaOH, KOH, RbOH, CsOH.

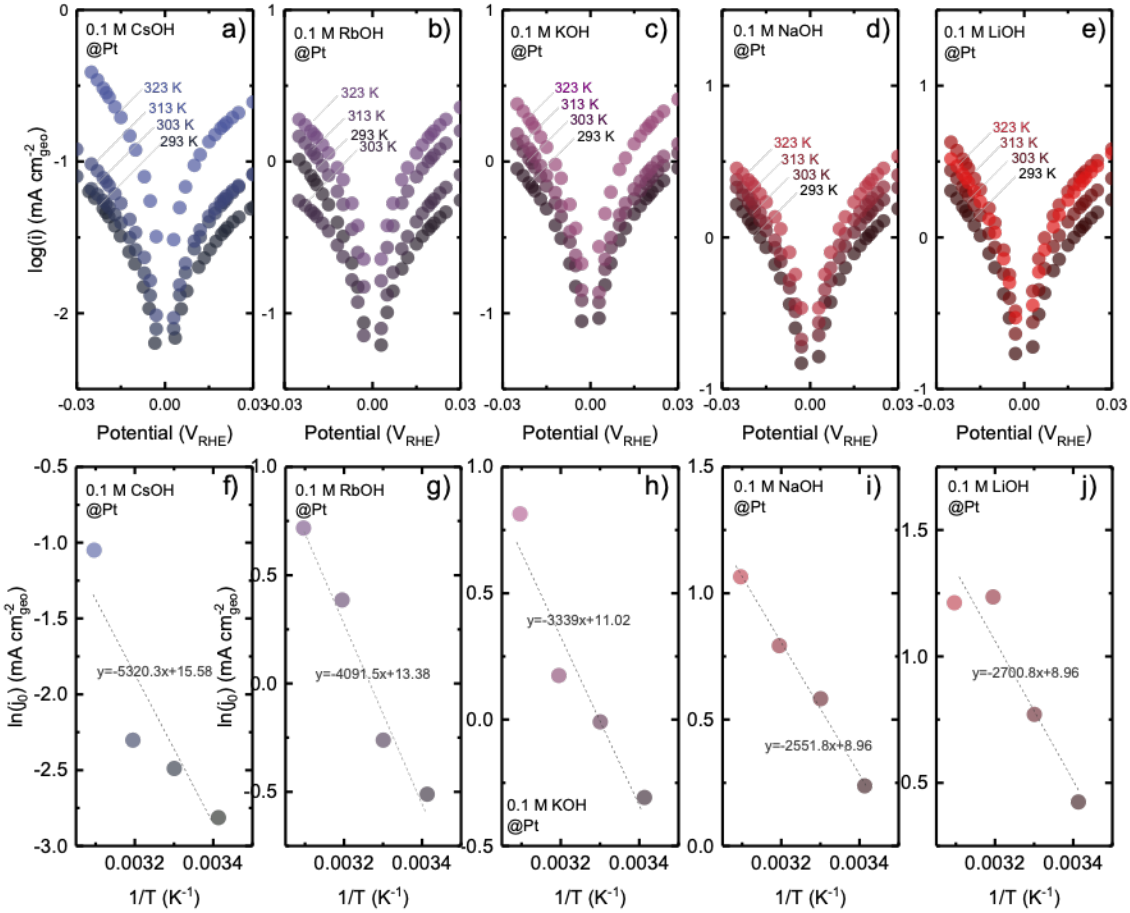

Figure S8. Estimation of the activation energy by Arrhenius plot. Temperature dependent kinetic current of HER/HOR in H_2-saturated aqueous solution at pH13 containing 0.1 M hydroxide of (**a**) Cs^+, (**b**) Rb^+, (**c**) K^+, (**d**) Na^+, (**e**) Li^+ on the Pt RDE electrode. Arrhenius plot of (**f**) Cs^+, (**g**) Rb^+, (**h**) K^+, (**i**) Na^+, (**j**) Li^+ cases.

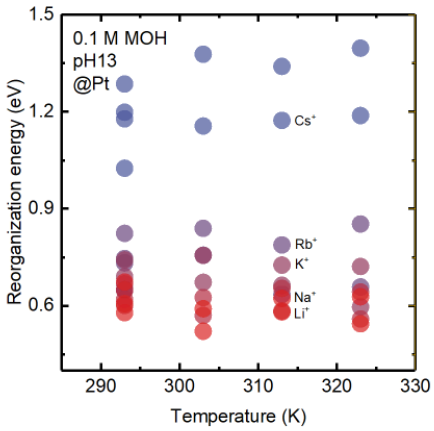

Figure S9. Reorganization energy of HER/HOR measured on Pt RDE at pH 13 in 0.1 M hydroxide of Li^+, Na^+, K^+, Rb^+ and Cs^+ for temperature range from 293 to 323 K by fitting temperature-dependent kinetics to MHC formalism with full data points of 2-3 independent measurements.

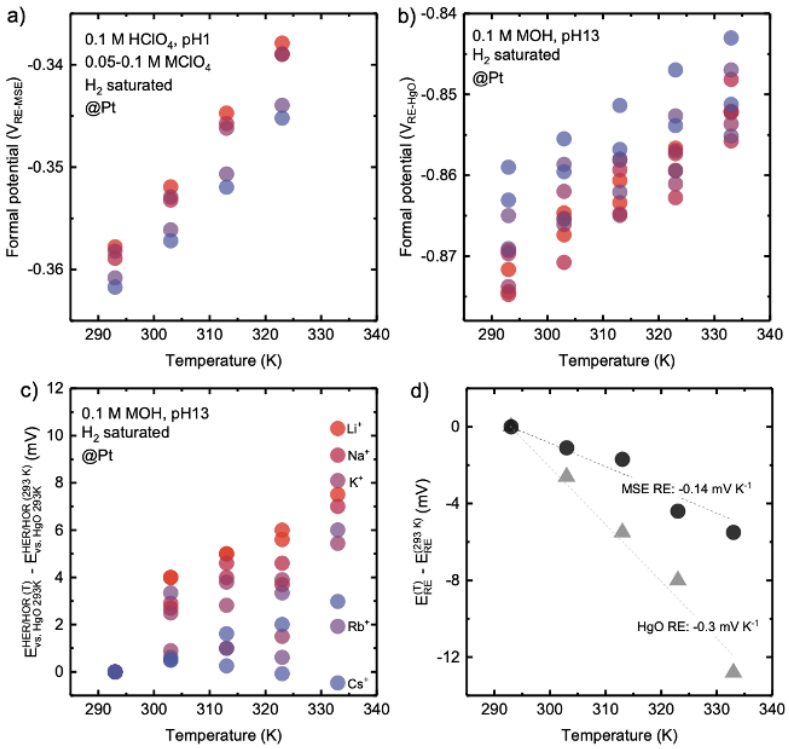

Figure S10. Cation- and pH-dependent formal potential of HER/HOR on Pt RDE at H_2 saturated electrolytes at pH1 and pH 13. (a) Temperature dependent HER/HOR potential (T) at pH 1 vs. $Hg/HgSO_4$ reference electrode at temperature T between 293 and 323 K; **(b)** Temperature dependent HER/HOR potential (T) at pH 13 vs. Hg/HgO reference electrode at temperature T between 293 and 333 K. **(c)** Temperature dependent HER/HOR potential (T) at pH 13 vs. the potential of Hg/HgO reference electrode at 293 K. **(d)** Temperature dependence of reference electrodes ($Hg/HgSO_4$ and Hg/HgO) potential from 293 to 333 K.

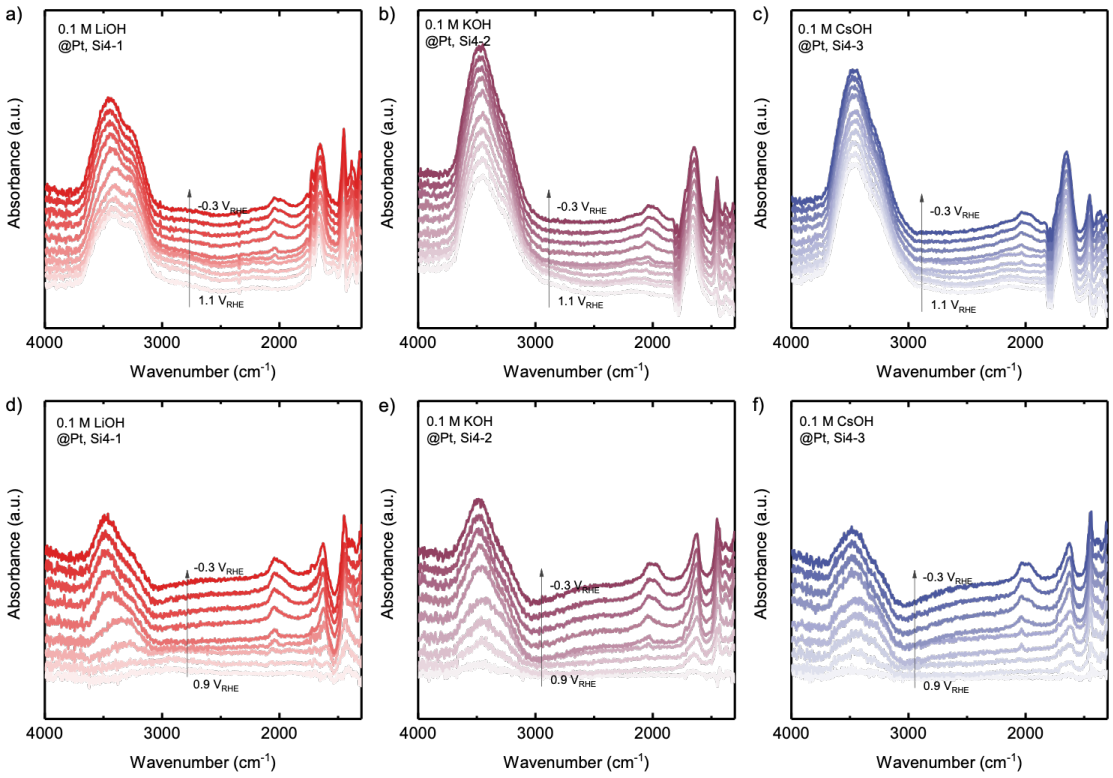

Figure S11. ***In situ*** **SEIRAS spectra of HER/HOR on Pt** measured from 1.1V_{RHE} to -0.3 V_{RHE} in an H_2 saturated aqueous solution of 0.1 M of **(a)** LiOH, (**b)** KOH and (**c)** CsOH. Spectra subtracted by the reference spectrum taken at 1.1 V_{RHE} for **(d)** LiOH, (**e)** KOH and **(f)** CsOH.

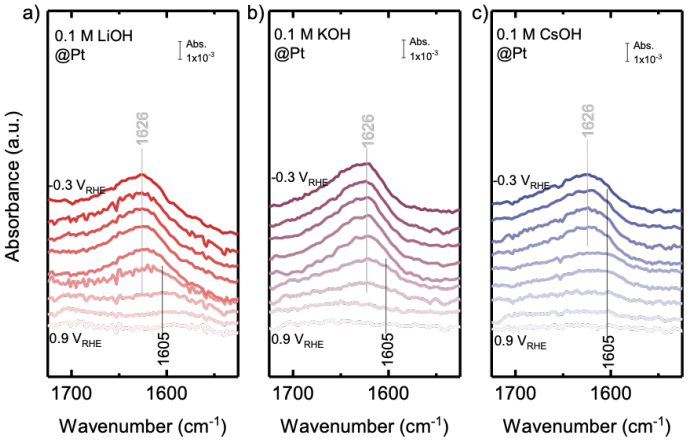

Figure S12. HOH bending feature of *in situ* SEIRAS spectra of HER/HOR on Pt measured from 1.1V_{RHE} to -0.3 V_{RHE} in an H_2 saturated aqueous solution of 0.1 M of (**a)** LiOH, (**b)** KOH and (**c)** CsOH. Spectra were subtracted by the reference spectrum taken at 1.1 V_{RHE}.

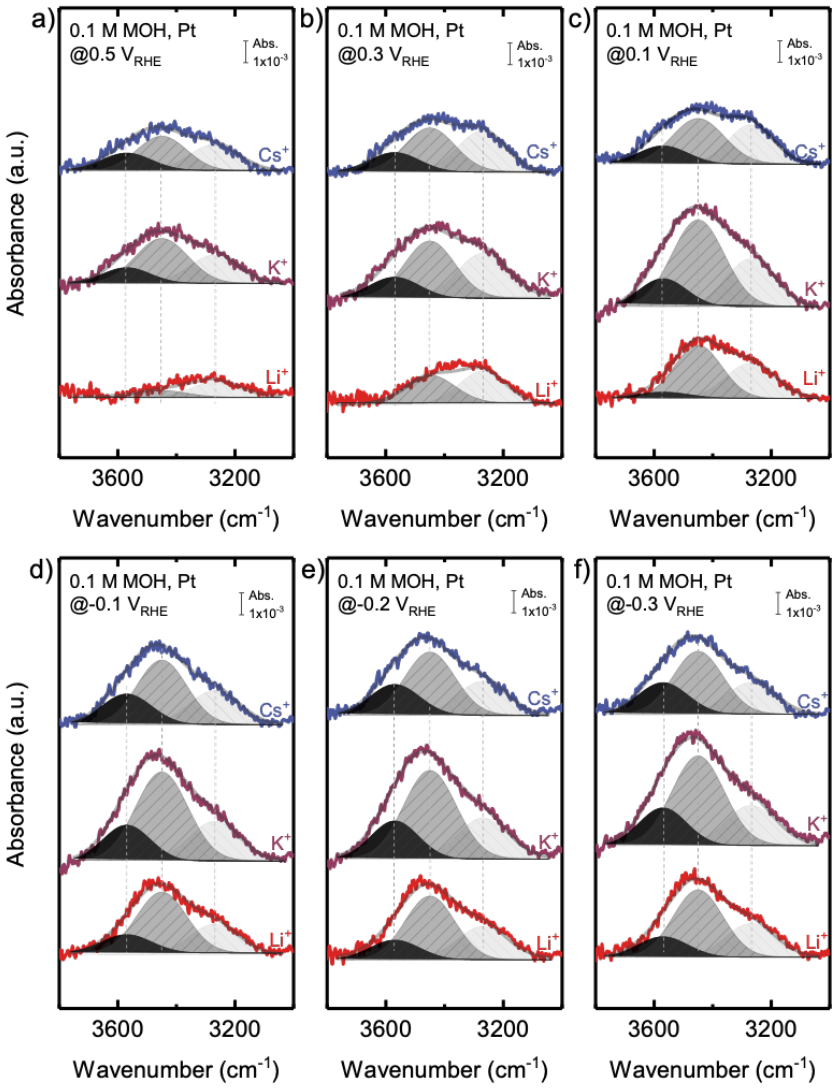

Figure S13. Deconvolution of OH stretching features of *in situ* SEIRAS spectra of HER/HOR on Pt measured from 1.1V_{RHE} to -0.3 V_{RHE} in an H_2 saturated aqueous solution of 0.1 M of LiOH, KOH and CsOH at **(a)** 0.5 V_{RHE}, **(b)** 0.3 V_{RHE}, **(c)** 0.1 V_{RHE}, **(d)** -0.1 V_{RHE}, **(e)** -0.2 V_{RHE}, and **(f)** -0.3 V_{RHE}. Spectra were subtracted by the reference spectrum taken at 1.1 V_{RHE}, the OH stretching peaks were deconvoluted into three components: 3570 cm^{-1} (weakly H-bonded /isolated water, black), 3450 cm^{-1} (asymmetric H-bonded water, dark grey), and 3270 cm^{-1} (symmetric H-bonded water, light grey).

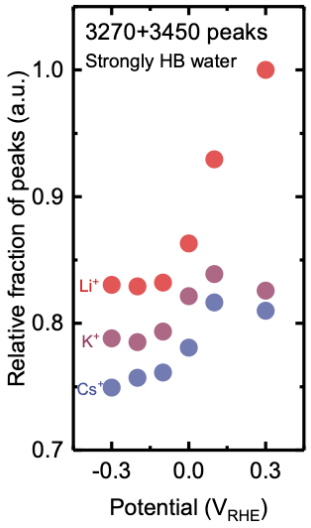

Figure S14. The potential-dependence of the relative fractions of strongly H-bonded water (asymmetric and symmetric H-bonded water molecules probed by OH stretching features of *in situ* SEIRAS spectra shown in Fig. S13.

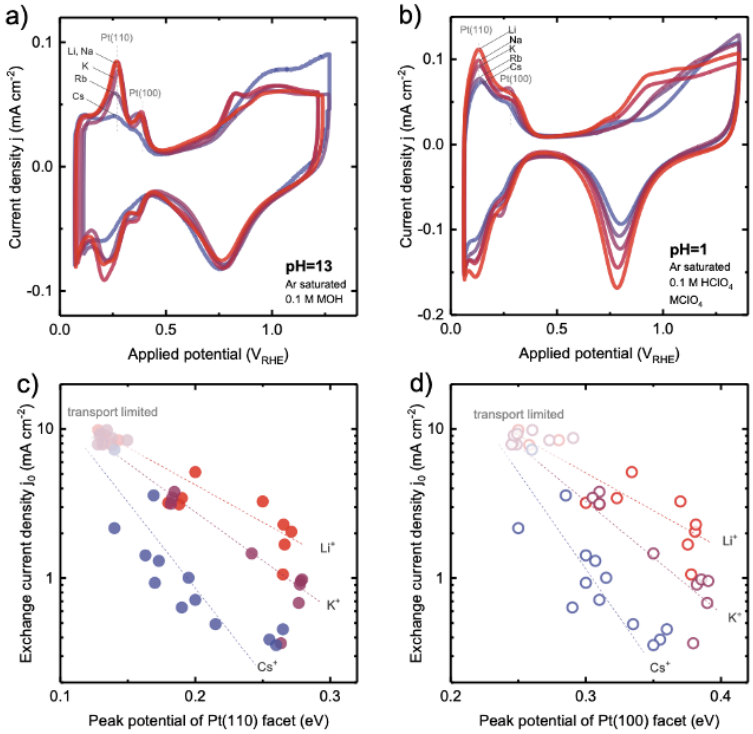

Figure S15. Cation effect on the H/OH exchange and HER/HOR kinetics at pH1 and pH13 on platinum RDE. (a) CV measured in Ar-saturated aqueous electrolytes of 0.1 M hydroxide of Li^+, Na^+, K^+, Rb^+ and Cs^+, **(b)** CV measured in Ar-saturated aqueous electrolytes of 0.1 M $HClO_4$ with 0.1 M perchlorate salts of Li^+, Na^+ or with 0.08 M perchlorate of K^+, Cs^+ or 0.05 M perchlorate of Rb^+. The plot of exchange current density j_0 of HER/HOR against the peak potential of H/OH exchange on **(c)** Pt (110) and **(d)** Pt(100) facets measured on polycrystalline Pt RDE in a wide range of electrolytes with pH ranging from 1 to 14: $HClO_4$ (pH=1-2), phosphoric acid buffer solutions (pH=1-13), citric acid buffer solutions (pH=1-3), acetic acid buffer solutions (pH=2-4), bicarbonate buffer solutions (pH=8-10), and KOH electrolytes (pH=12-14). Note that mass transport limitation in HER/HOR on Pt RDE measurements underestimates the exchange current density > ~6 $mA\ cm_{geo}^{-2}$, which is shaded (Fig. S4).

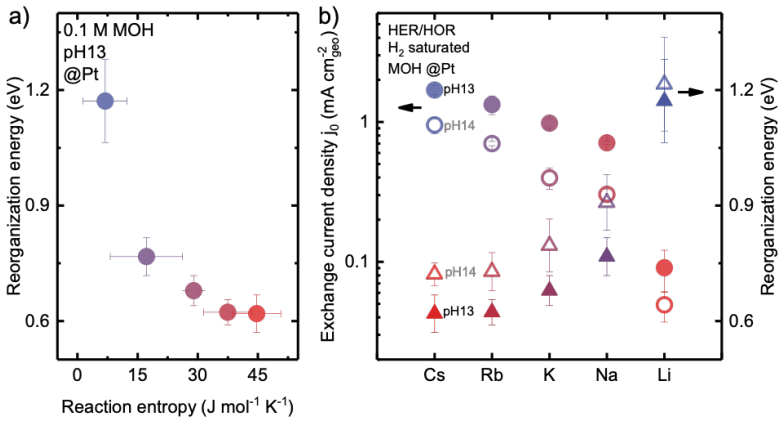

Figure S16. (a) Correlation between reorganization energy and reaction entropy change of HER/HOR on Pt RDE at pH 13 measured in H_2 saturated 0.1 M hydroxide of Li^+, Na^+, K^+, Rb^+ and Cs^+. **(b)** Cation-dependent exchange current density and reorganization energy of HER/HOR on Pt RDE at pH 13 and pH14.

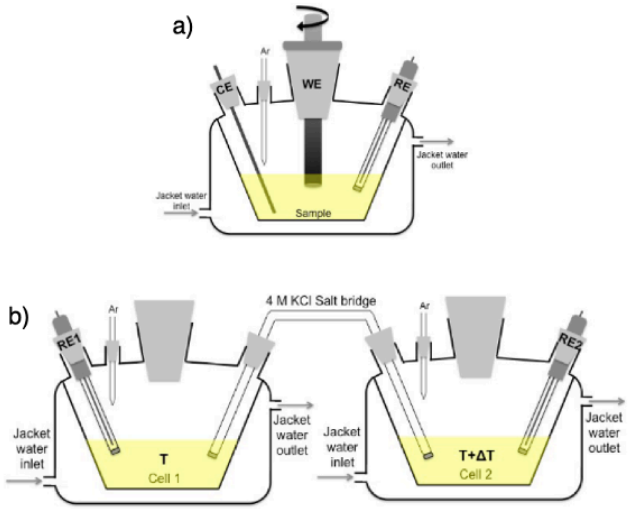

Figure S17. Schematic of electrochemical cells for kinetics and reaction entropy measurements. **a)** Isothermal cell for kinetic and reaction entropy measurements, **b)** non-isothermal cell for the calibration of the temperature coefficient of reference electrode.

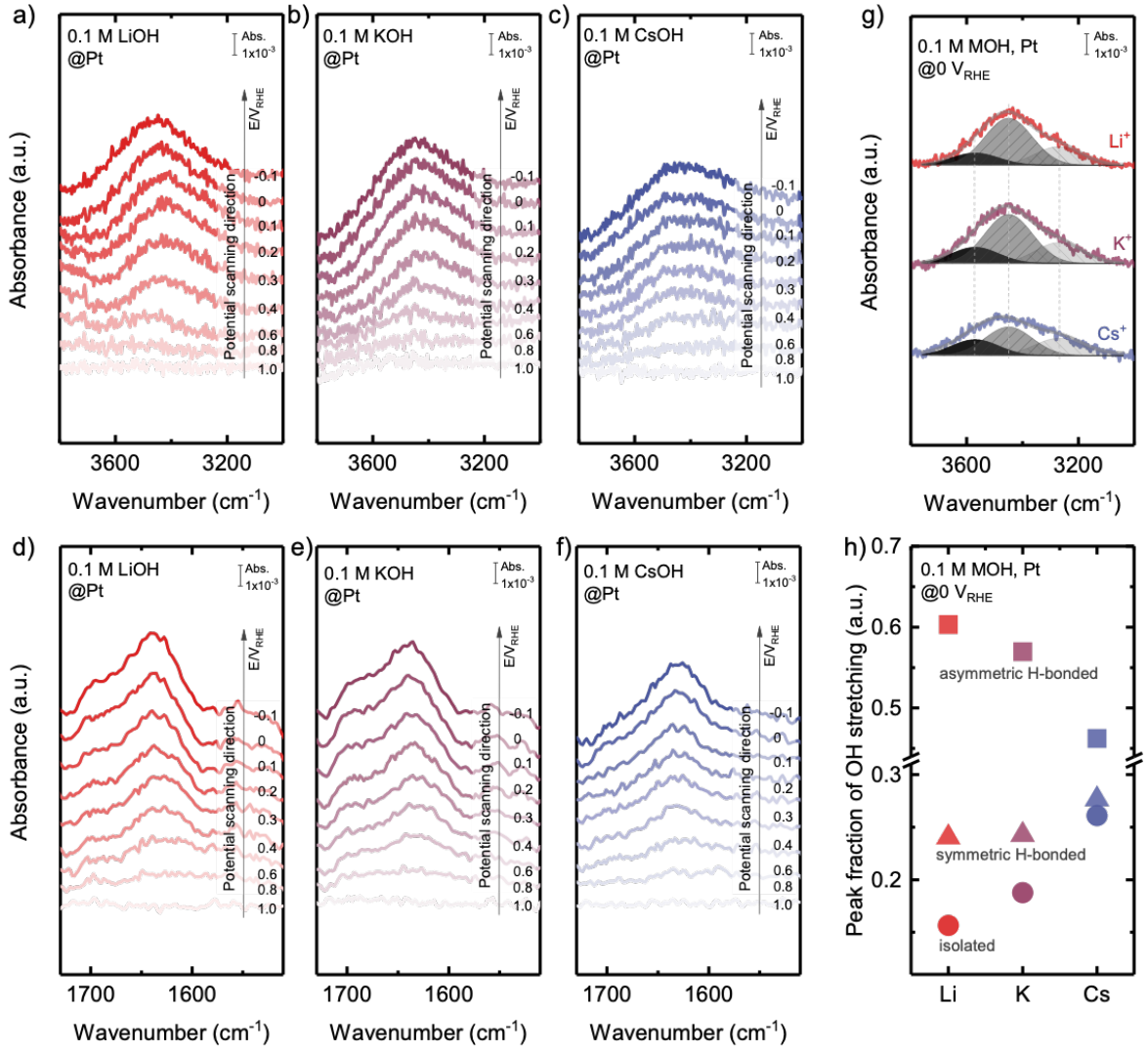

Figure S18. 2nd run of *in situ* SEIRAS spectra of HER/HOR on Pt measured from 1.1V_{RHE} to -0.1 V_{RHE} in an H_2 saturated aqueous solution of 0.1 M of hydroxide of Li^+, K^+ and Cs^+., where spectra were subtracted by the reference spectrum taken at 1.1 V_{RHE}. OH stretching region for (**a**) LiOH, (**b**) KOH and (**c**) CsOH. HOH bending region for (**d**) LiOH, (**e**) KOH and (**f**) CsOH. (**g**) Deconvolution of OH stretching peak at 0 V_{RHE} into three components: 3570 cm^{-1} (weakly H-bonded /isolated water), 3450 cm^{-1} (asymmetric H-bonded water), and 3270 cm^{-1} (symmetric H-bonded water). (**h**) the relative fractions of isolated water, asymmetric H-bonded water and symmetric H-bonded water from spectra shown in Fig. S18g.

Table S1. Summary of force field parameters used in the simulations.

	σ [Å]	ϵ [$kcal/mol$]	$Charge$ [e]
SPC/E Water[2]			
O	3.166	0.1553	-0.8476
H	-	-	+0.4238
Alkali Ions[29,30]			
Li^+	1.715	0.05766	+0.94
Na^+	2.497	0.07826	+0.94
K^+	3.184	0.1183	+0.94
Rb^+	3.302	0.2405	+0.94
Cs^+	3.440	0.5013	+0.94
Counter Ion[29,30]			
Cl^-	4.612	0.02502	-0.94
Pt Electrode[3,4]			
Pt	2.535	7.80	†

† The charges on the platinum electrode atoms are calculated at each time step by the LAMMPS constant potential fix developed by Wang et al.[4]

Table S2. Probing impurities in CsOH solution 50 wt. % in water and 99.95% trace metals basis as received by using inductively coupled plasma.

Elements	Concentration (ppm)	Mass percentage (%)
Cs	257722.46	99.95
Rb	29.42	0.01
K	31.6	0.01
Na	28.14	0.01
Li	4.03	0
Ag	0	0
Al	4.69	0
B	1.09	0
Ba	28.00	0.01
Bi	0	0
Ca	0	0
Cd	0	0
Co	0	0
Cr	0	0
Cu	0	0
Fe	0	0
Mg	0	0
Mn	0	0
Mo	0.22	0
Ni	0.11	0
Pb	0	0
Sr	1.53	0
Tl	0	0
Zn	0.4	0

Appendix S1: Justification of the application of Marcus-Hush-Chidsey (MHC) model during proton coupled electron transfer

The Marcus theory describes that the solvent plays a crucial role in all electrochemical reactions involving electron transfer, which indicates that realistic calculations would have to include a fair amount of water molecules at the electrochemical interface and also need to consider the surface charge and the applied potential of the electrode simultaneously. As mentioned by the reviewer, Schmickler's model is the one of famous theoretical frameworks for illustrating the kinetics of proton discharge on metal surface (Volmer step), which combines the key ideas of the Marcus theory,[31] Anderson-Newns model[32,33] and the tight binding theory.[17] The total model Hamiltonian of this system is defined as the sum of the two components from electrode and solvent, $H_{el}+H_{sol}$. Base on the Anderson-Newns model, the model Hamiltonian of electrode (H_{el}) considering electron transfer between 1s orbital of hydrogen atom and metal electrode could be calculated as following: [17]

$$H_{\mathrm{el}} = \epsilon_a n_a + \sum_k \epsilon_k c_k + \sum_k [V_k c_k^+ c_a + V_k^* c_a^+ c_k].$$

where the index a represents the hydrogen 1s orbital, ϵ_a is its energy, and n_a the corresponding number operator; the metal states are labeled k and thus have energies ϵ_k and number operators n_k. The last term affects electron exchange between the metal and the reactant; c^+ denotes a creation and c is an annihilation operator. On the other hand, the Hamiltonian of solvent (H_{sol}) can be deduced based on the Marcus theory as following:

$$H_{\mathrm{sol}} = \frac{1}{2}\sum_\nu \hbar\omega_\nu(q_\nu^2 + p_\nu^2) + (1 - n_a)\sum_\nu \hbar\omega_\nu g_\nu q_\nu.$$

where ν labels the phonon modes, q_ν and p_ν are the dimensionless coordinate and momentum operators for the modes with frequencies ω_υ, and in the last term g_ν is the interaction constant of the charge with the mode. The interaction of the solvent with the reactant is characterized by the energy of reorganization $\lambda = \Sigma_\nu \hbar\omega_\nu g_\nu^2/2$. Although the Schmickler's model can consider the reactant/electrode interaction and solvent effect simultaneously, it is too complicated to be used to analyze results generated from experiments. Therefore, previous work[34] has used the effect of d band position of metal to describe the interaction between d band of metal and 1s orbital of H atom. Furthermore, the interaction of the reactant with the solvent can be significantly larger than that between reactant and electrode, particularly in the case of proton, having a hydration energy of 11.5 eV[17] which is two orders of magnitude larger than HBE on Pt (-0.1 eV).[18] Therefore, the reactant/solvent interaction is important in controlling kinetics of proton coupled electron transfer (PCET) processes. In this manuscript, we studied the HER kinetics on Pt, which is a PCET, the analysis and discussion therefore focus on the reactant/solvent interaction (H_{sol}) based on the Marcus theory to extract reorganization energy.

Although, the interaction of reactant and electrode is not considered in the Marcus-Hush-Chidsey (MHC) model, where the Fermi-Dirac distribution of electrons is incorporated, it has been reported to accurately predict activity trends of numerous Faradaic reaction kinetics, for example, PCET reactions (HER/HOR on nickel-based molecular electrocatalyst[12] and the reduction of water-superoxide ion complex on glassy carbon electrode[13]), interfacial ET on the metal surfaces,[14] lithium electrodeposition/stripping[15] and lithium-ion intercalation at solid-solid interfaces.[9,16] Therefore, we propose that MHC formalism might be used to analyze the kinetics of PCET such as HER/HOR. This hypothesis is supported by the fact that the values of exchange current density extracted by MHC formalism (Figs S2a,c) are comparable to those extracted via Butler-Volmer equation (Figs S2b,c). Further support comes from that the values

of the reorganization energy of the Volmer reaction on metal surface has been reported to be ~0.4 eV,[19] which is comparable to the cation-dependent reorganization energy found in this work, 0.6-1.2 eV. Therefore, based on our learnings from the literature (refs [13,20–22]) and the consistency between our results and previous work (refs [12,23]), we propose that the kinetics of HER/HOR on Pt RDE can be described by the MHC formalism.

Appendix S2: Reaction entropy change of redox reactions[6]

The redox reaction entropy Δs can be estimated by the temperature dependence of the formal potential $E^{0\prime}$ of the redox couple:

$$\Delta S = nF\frac{dE^{0\prime}(T)}{dT}$$

F is the Faraday constant and *n* is the number of electrons involved in the corresponding redox process. The ratio $dE^{0\prime}/dT$ is also called the temperature coefficient of the redox couples, denoted by α:

$$\alpha = \frac{dE^{0\prime}(T)}{dT}$$

In an isothermal electrochemical cell (Fig. S17a), potentials are referenced to a reference electrode (RE), thus:

$$E^{0\prime}(T) = E_{meas}(T) + E_{RE}(T)$$

$E_{meas}(T)$ is the measured potential at the working electrode (WE); $E_{RE}(T)$ is the potential of the RE at temperature T. Then, the redox reaction entropy Δs can be expressed as,

$$\Delta S = nF\left[\frac{dE_{meas}(T)}{dT} + \frac{dE_{RE}(T)}{dT}\right] = nF(\alpha_{meas} + \alpha_{RE})$$

The temperature coefficients of reference electrodes (RE) α_{RE}, $Hg/HgSO_4$ RE for acidic and neutral electrolytes, and Hg/HgO RE for alkaline electrolytes, were calibrated using a non-isothermal cell set-up (**Fig. S17b**). Two independently thermostated cells (cell 1 and 2) were filled with 4 M KCl electrolyte and connected by a 4 M KCl salt bridge. Two RE were used and inserted in the cells. For calibrating RE2, the change of the electromotive force $dE_{RE2}(T)$ between RE2 and RE1 upon an increase of temperature difference at the two compartments was measured (the temperature of cell 1 was maintained at 22°C whereas that of cell 2 increased from 20°C to 60°C by an increment of 10°C). The temperature coefficient of the RE2 corresponds to the slope of the plot of $dE_{RE2}(T)$ against dT. The calibration of $Hg/HgSO_4$ and Hg/HgO REs is shown in **Fig. S10d**.

Appendix S3: Potential of zero charge of Pt surfaces

The measurement of PZC of Pt surfaces can be interfered by the adsorption processes (H_{ad} and OH_{ad}) that involve charge transfer. It turns out that it is impossible to unambiguously discriminate only from macroscopic electrochemical measurements whether there is a true charge separation at the interface (true capacitive charge) from a situation where charge has been redistributed to form covalent bonds between the surface and the adsorbed species (pseudocapacity phenomena).[35] In this regards, it is necessary to distinguish between the potential of zero free charge (PZFC), the true electronic excess charge on the metal balanced by ionic charge in the electrolyte, and the potential of zero total charge (PZTC), which includes both the capacitive and the faradaic charge. [35] Consequently, with these definitions there will be two different values of PZC: PZFC and PZTC. The first one is that related with the structural microscopic properties of the interface, such as work function, dipole orientation, etc. and is equivalent to the PZC in non-hydrogen adsorbing metals. However, the latter is the only one accessible from electrochemical measurements. The CO displacement experiment allowed determining the potential at which the displaced charge is zero, which was considered as a measure of the PZTC of the interface as a first approximation. Considering the work by Rizo et al. [35], Chen et al. [36] and Domke et al. [37], the PZFC and PZTC on Pt polycrystalline, single crystal and stepped surfaces at pH1 showed similar values, ~0.3-0.4 V_{RHE}. Although the values of the PZFC and PZTC of Pt(111) at pH13 differed from each other, 0.7 V_{RHE} for PZTC and 1.05 V_{RHE} for PZFC, the pH dependence of PZTC/PZFC was consistent, where PZTC/PZFC increases with increasing pH.

Rizo et al. [35]

Facets	**pH**	**PZTC (V_{RHE})**	**PZFC (V_{RHE})**
Pt(111)	13.1	0.7	1.05
	12.3	0.68	1.01
	11.1	0.69	0.94
	8.4	0.62	0.78
	3.4	0.48	0.48
	2.3	0.44	0.42
	1.2	0.39	0.34

Chen et al. [36]

Facets	**pH**	**PZTC (V_{RHE})**	**PZFC (V_{RHE})**
Pt polycrystalline	1	0.29	-
Pt(100)	1	0.34	-
Pt(100-111)	1	0.31	-
Pt(111)	1	0.28	-

Domke et al. [37]

Facets	**pH**	**PZTC (V_{RHE})**	**PZFC (V_{RHE})**
Pt(311)	1	0.41	-
Pt(511)	1	0.41	-
Pt(711)	1	0.41	-
Pt(11,1,1)	1	0.39	-
Pt(19,1,1)	1	0.37	-
Pt(29,1,1)	1	0.35	-
Pt(29,1,1)	1	0.33	-

Appendix S4: Activity coefficient of hydroxide anion at the Pt interface

The reaction entropy of HER/HOR was estimated from the temperature-dependent potential change, $\Delta S = \frac{dE(T)}{dT} = nF\left[\frac{dE_{meas}(T)}{dT} + \frac{dE_{RE}(T)}{dT}\right]$ (Appendix S2), where the electrode potential could be described using Nernst Equation, $E = E^0 - \frac{RT}{nF} ln \frac{P_{H2} \cdot (\gamma_{OH^-} \cdot [OH^-])^2}{(\gamma_{H2O} \cdot [H_2O])^2}$ with γ_i represent the activity coefficient of specie *i*. Since entropy is a thermodynamic state variable, any difference in the entropy of reaction between hydroxide of alkali cations could originate from a difference in the activity coefficient.

Here, we illustrate the influence of cations on the activity coefficient of OH^-. For the first approximation, we consider the extended Debye-Hückel equation[38] for ionic strength < 0.1 M, where the activity coefficient could be written as following:

$$log\gamma_{OH^-} = -A \cdot Z_{OH^-}^2 \cdot \frac{\sqrt{I}}{1 + B \cdot r_{OH^-} \cdot \sqrt{I}}$$

With

$$A = \frac{e^2 B}{2.303 \times 8\pi\epsilon_0\epsilon_r k_B T}$$

$$B = \sqrt{\frac{2e^2 N_A}{\epsilon_0\epsilon_r k_B T}}$$

where A and B are constants that depends on temperature *T*; r_{OH^-} and Z_{OH^-} are the effective radii and charge of OH^-; *I* is the ionic strength; *e* is the elementary charge; ϵ_0 is the permittivity of vacuum; ϵ_r is the relative permittivity; k_B and N_A is the Boltzmann and Avogadro constants.

By considering the parameters from the current manuscript, e.g. the effective ionic radii of OH^- in the order of Li^+ (1.6 å) < Na^+ (1.7 å) < K^+ (1.9 å) < Rb^+ (2.1 å) < Cs^+ (2.4 å) and interfacial static dielectric constant in the order of Li^+ (2.6) ~ Na^+ (2.6) < K^+ (2.7) < Rb^+ (2.9) < Cs^+ (4.3), the values of OH^- activity coefficient in 0.1 M hydroxide electrolyte were found be to be in the order of Li^+ (0.15) ~ Na^+ (0.15) < K^+ (0.16) < Rb^+ (0.19) < Cs^+ (0.4) via the extended Debye-Hückel equation.

As the application of the extended Debye-Hückel equation could be more suitable for solution at ionic strength smaller than 0.1 M, we further tried to estimate the activity coefficient using Davies equation,[39] which allows to estimate the activity coefficient for solutions at ionic strength lower than 0.5 M.

$$log\gamma_{OH^-} = -A \cdot Z_{OH^-}^2 \cdot \left(\frac{\sqrt{I}}{1 + \sqrt{I}} - 0.3 \cdot I\right)$$

Similar to the extended Debye-Hückel equation, the Davies equation gave the activity coefficient of OH^- in the order of Li^+ (0.21) ~ Na^+ (0.21) < K^+ (0.23) < Rb^+ (0.27) < Cs^+ (0.48).

Both the extended Debye-Hückel and the Davies equations showed that the activity coefficient of OH^- at the interface was lower than that estimated at bulk solution, being 0.94 for the extended Debye-Hückel equation and 0.96 for the Davies equation.

The results shows that the values of the activity coefficient of OH^- varies from 0.21 for Li^+ to 0.48 for Cs^+, which is smaller than those reported by Harned and Swindells,[40] being 0.79 for KOH, 0.78 for NaOH and 0.75 for CsOH, for centration at 0.1 M hydroxide solutions. Although

the absolute values of OH^- activity coefficient differ between our work and Harned and Swindells's work,[40] the cation dependent trends are the same, the activity coefficient of OH^- increases with increasing cation radii.

We further estimated the Gibbs free energy of the reaction ΔG ($\Delta G = \Delta G_{OH^-} - \Delta G_{H_2O}$), where the change of the Gibbs free energy ΔG of OH^- for Li^+ and Cs^+, which should change by a factor of $-2.303 \cdot R \cdot T \cdot Log(\gamma_{OH^-})$ according to Nernst Equation. The values of $2.303 \cdot R \cdot T \cdot Log(\gamma_{OH^-})$ can be estimated to be -0.038 eV for Li^+ and -0.018 eV for Cs^+. Between the two extreme cations (Li^+ and Cs^+), the Gibbs free energy of the reaction ΔG varies by 0.02 eV whereas the free energy of activation $\Delta G^{\neq}$ increases 0.23 eV (from 0.23 eV for Li^+ to 0.46 eV for Cs^+, Fig. 4b). The comparison of the Gibbs free energy of the reaction ΔG and the free energy of activation $\Delta G^{\neq}$ shows that the barrier of kinetics can be 1 order of magnitude larger than the thermodynamic driving force, the Gibbs free energy of the reaction ΔG. The proportionality between the Gibbs free energy of the reaction ΔG and the free energy of activation $\Delta G^{\neq}$ indicates that the linear free energy relationship holds and could explain the cation dependent HER/HOR kinetics at pH 13 in this work.

References

(1) Hockney, R. W.; Eastwood, J. W. *Computer Simulation Using Particles*, 1st ed.; Taylor & Francis, Inc.: Philadelphia, 1988.
(2) Berendsen, H. J. C.; Grigera, J. R.; Straatsma, T. P. The Missing Term in Effective Pair Potentials. *The Journal of Physical Chemistry* **1987**, *91* (24), 6269–6271.
(3) Heinz, H.; Vaia, R. A.; Farmer, B. L.; Naik, R. R. Accurate Simulation of Surfaces and Interfaces of Face-Centered Cubic Metals Using 12−6 and 9−6 Lennard-Jones Potentials. *The Journal of Physical Chemistry C* **2008**, *112* (44), 17281–17290.
(4) Wang, Z.; Yang, Y.; Olmsted, D. L.; Asta, M.; Laird, B. B. Evaluation of the Constant Potential Method in Simulating Electric Double-Layer Capacitors. *The Journal of Chemical Physics* **2014**, *141* (18), 184102.
(5) Yamakata, A.; Osawa, M. Destruction of the Water Layer on a Hydrophobic Surface Induced by the Forced Approach of Hydrophilic and Hydrophobic Cations. *J. Phys. Chem. Lett.* **2010**, *1* (9), 1487–1491.
(6) Huang, B.; Muy, S.; Feng, S.; Katayama, Y.; Lu, Y.-C.; Chen, G.; Shao-Horn, Y. Non-Covalent Interactions in Electrochemical Reactions and Implications in Clean Energy Applications. *Phys. Chem. Chem. Phys.* **2018**, *20* (23), 15680–15686.
(7) Bard, A. J.; Faulkner, L. R. *ELECTROCHEMICAL METHODS Fundamentals and Applications*, 2nd ed.; John Wiley & Sons, INC: New York.
(8) Zeng, Y.; Smith, R. B.; Bai, P.; Bazant, M. Z. Simple Formula for Marcus–Hush–Chidsey Kinetics. *Journal of Electroanalytical Chemistry* **2014**, *735*, 77–83.
(9) Bai, P.; Bazant, M. Z. Charge Transfer Kinetics at the Solid–Solid Interface in Porous Electrodes. *Nature Communications* **2014**, *5*, 3585.
(10) Marcus, R. A.; Sutin, N. Electron Transfers in Chemistry and Biology. *Biochimica et Biophysica Acta (BBA) - Reviews on Bioenergetics* **1985**, *811* (3), 265–322.
(11) Marcus, R. A. On the Theory of Oxidation-Reduction Reactions Involving Electron Transfer. I. *The Journal of Chemical Physics* **1956**, *24*, 966.
(12) Horvath, S.; Fernandez, L. E.; Soudackov, A. V.; Hammes-Schiffer, S. Insights into Proton-Coupled Electron Transfer Mechanisms of Electrocatalytic H_2 Oxidation and Production. *Proc Natl Acad Sci USA* **2012**, *109* (39), 15663.
(13) Costentin, C.; Evans, D. H.; Robert, M.; Savéant, J.-M.; Singh, P. S. Electrochemical Approach to Concerted Proton and Electron Transfers. Reduction of the Water−Superoxide Ion Complex. *J. Am. Chem. Soc.* **2005**, *127* (36), 12490–12491.
(14) Huang, B.; Myint, K. H.; Wang, Y.; Zhang, Y.; Rao, R. R.; Sun, J.; Muy, S.; Katayama, Y.; Corchado Garcia, J.; Fraggedakis, D.; Grossman, J. C.; Bazant, M. Z.; Xu, K.; Willard, A. P.; Shao-Horn, Y. Cation-Dependent Interfacial Structures and Kinetics for Outer-Sphere Electron-Transfer Reactions. *J. Phys. Chem. C* **2021**, *125* (8), 4397–4411.
(15) Boyle, D. T.; Kong, X.; Pei, A.; Rudnicki, P. E.; Shi, F.; Huang, W.; Bao, Z.; Qin, J.; Cui, Y. Transient Voltammetry with Ultramicroelectrodes Reveals the Electron Transfer Kinetics of Lithium Metal Anodes. *ACS Energy Lett.* **2020**, *5* (3), 701–709.
(16) Fraggedakis, D.; McEldrew, M.; Smith, R. B.; Krishnan, Y.; Zhang, Y.; Bai, P.; Chueh, W. C.; Shao-Horn, Y.; Bazant, M. Z. Theory of Coupled Ion-Electron Transfer Kinetics. *Electrochimica Acta* **2021**, *367*, 137432.
(17) Santos, E.; Lundin, A.; Pötting, K.; Quaino, P.; Schmickler, W. Model for the Electrocatalysis of Hydrogen Evolution. *Phys. Rev. B* **2009**, *79* (23), 235436.
(18) Greeley, J.; Jaramillo, T. F.; Bonde, J.; Chorkendorff, I.; Nørskov, J. K. Computational High-Throughput Screening of Electrocatalytic Materials for Hydrogen Evolution. *Nature Materials* **2006**, *5* (11), 909–913.
(19) Lam, Y.-C.; Soudackov, A. V.; Hammes-Schiffer, S. Theory of Electrochemical

Proton-Coupled Electron Transfer in Diabatic Vibronic Representation: Application to Proton Discharge on Metal Electrodes in Alkaline Solution. *J. Phys. Chem. C* **2020**, *124* (50), 27309–27322.
(20) Marcus, R. A. Electron Transfer Reactions in Chemistry: Theory and Experiment (Nobel Lecture). *Angewandte Chemie International Edition in English* **1993**, *32* (8), 1111–1121.
(21) Henstridge, M. C.; Laborda, E.; Rees, N. V.; Compton, R. G. Marcus–Hush–Chidsey Theory of Electron Transfer Applied to Voltammetry: A Review. *Electrochimica Acta* **2012**, *84*, 12–20.
(22) CHIDSEY, C. E. D. Free Energy and Temperature Dependence of Electron Transfer at the Metal-Electrolyte Interface. *Science* **1991**, *251* (4996), 919.
(23) Sheng, W.; Zhuang, Z.; Gao, M.; Zheng, J.; Chen, J. G.; Yan, Y. Correlating Hydrogen Oxidation and Evolution Activity on Platinum at Different PH with Measured Hydrogen Binding Energy. *Nature Communications* **2015**, *6*, 5848.
(24) Peter, L. M.; Dürr, W.; Bindra, P.; Gerischer, H. The Influence of Alkali Metal Cations on the Rate of the Fe(CN)64−/Fe(CN)63− Electrode Process. *Journal of Electroanalytical Chemistry and Interfacial Electrochemistry* **1976**, *71* (1), 31–50.
(25) Katayama, Y.; Okanishi, T.; Muroyama, H.; Matsui, T.; Eguchi, K. Enhanced Supply of Hydroxyl Species in CeO2-Modified Platinum Catalyst Studied by in Situ ATR-FTIR Spectroscopy. *ACS Catal.* **2016**, *6* (3), 2026–2034.
(26) Katayama, Y.; Giordano, L.; Rao, R. R.; Hwang, J.; Muroyama, H.; Matsui, T.; Eguchi, K.; Shao-Horn, Y. Surface (Electro)Chemistry of CO2 on Pt Surface: An in Situ Surface-Enhanced Infrared Absorption Spectroscopy Study. *J. Phys. Chem. C* **2018**, *122* (23), 12341–12349.
(27) Nakamura, M.; Nakajima, Y.; Hoshi, N.; Tajiri, H.; Sakata, O. Effect of Non-Specifically Adsorbed Ions on the Surface Oxidation of Pt(111). *ChemPhysChem* **2013**, *14* (11), 2426–2431.
(28) Sheng, W.; Gasteiger, H. A.; Shao-Horn, Y. Hydrogen Oxidation and Evolution Reaction Kinetics on Platinum: Acid vs Alkaline Electrolytes. *Journal of The Electrochemical Society* **2010**, *157* (11), B1529–B1536.
(29) Mao, A. H.; Pappu, R. V. Crystal Lattice Properties Fully Determine Short-Range Interaction Parameters for Alkali and Halide Ions. *The Journal of Chemical Physics* **2012**, *137* (6), 64104.
(30) Kann, Z. R.; Skinner, J. L. A Scaled-Ionic-Charge Simulation Model That Reproduces Enhanced and Suppressed Water Diffusion in Aqueous Salt Solutions. *Journal of Chemical Physics* **2014**, *141* (10).
(31) Marcus, R. A. On the Theory of Electron-Transfer Reactions. VI. Unified Treatment for Homogeneous and Electrode Reactions. *J. Chem. Phys.* **1965**, *43* (2), 679–701.
(32) Anderson, P. W. Localized Magnetic States in Metals. *Phys. Rev.* **1961**, *124* (1), 41–53.
(33) Newns, D. M. Self-Consistent Model of Hydrogen Chemisorption. *Phys. Rev.* **1969**, *178* (3), 1123–1135.
(34) Santos, E.; Schmickler, W. Electrocatalysis of Hydrogen Oxidation—Theoretical Foundations. *Angewandte Chemie International Edition* **2007**, *46* (43), 8262–8265.
(35) Rizo, R.; Sitta, E.; Herrero, E.; Climent, V.; Feliu, J. M. Towards the Understanding of the Interfacial PH Scale at Pt(111) Electrodes. *Electrochimica Acta* **2015**, *162*, 138–145.
(36) Chen, Q.-S.; Solla-Gullón, J.; Sun, S.-G.; Feliu, J. M. The Potential of Zero Total Charge of Pt Nanoparticles and Polycrystalline Electrodes with Different Surface Structure: The Role of Anion Adsorption in Fundamental Electrocatalysis. *Electrochimica Acta* **2010**, *55* (27), 7982–7994.

(37) Domke, K.; Herrero, E.; Rodes, A.; Feliu, J. M. Determination of the Potentials of Zero Total Charge of Pt(100) Stepped Surfaces in the [01$\bar{1}$] Zone. Effect of the Step Density and Anion Adsorption. *Journal of Electroanalytical Chemistry* **2003**, *552*, 115–128.
(38) Garrels, R. M.; Gucker, F. T. Activity Coefficients and Dissociation of Lead Chloride in Aqueous Solutions. *Chem. Rev.* **1949**, *44* (1), 117–134.
(39) King, E. L. Ion Association. *Science* **1964**, *143* (3601), 37.
(40) Harned, H. S.; Swindells, F. E. THE ACTIVITY COEFFICIENT OF LITHIUM HYDROXIDE IN WATER AND IN AQUEOUS LITHIUM CHLORIDE SOLUTIONS, AND THE DISSOCIATION OF WATER IN LITHIUM CHLORIDE SOLUTIONS. *J. Am. Chem. Soc.* **1926**, *48* (1), 126–135.